Supplement of Atmos. Chem. Phys., 25, 14747–14762, 2025
https://doi.org/10.5194/acp-25-14747-2025-supplement

Atmospheric Chemistry and Physics
Open Access

Supplement of

Optimizing ammonia emissions for $PM_{2.5}$ mitigation: environmental and health co-benefits in Eastern China

Keqin Tang et al.

Correspondence to: Nan Li (linan@nuist.edu.cn)

Section S1

For surface NH_3 volume concentrations, we extracted the corresponding simulations at 12 sites summarized from previous in situ measurement studies and conducted a comparison between the model simulations and the measurements in terms of the annual mean NH_3 volume concentrations.

For comparison with IASI satellite retrievals, the total vertical column density (VCD) was calculated from the model's layer-specific output. The WRF-Chem model outputs NH_3 concentrations as a volume mixing ratio (in ppmv) for each model layer. To convert these layer-specific concentrations into a VCD, the subsequent process was followed.

First, the thickness of each model layer (ΔZ) must be determined. As our WRF-Chem setup uses a terrain-following hybrid sigma-pressure coordinate system, the geopotential height (Z) of each model level is calculated from the model's perturbation geopotential (PH) and base-state geopotential (PHB), divided by the acceleration due to gravity ($g \approx 9.8$ m s^{-2}):

$$Z = \frac{PH + PHB}{g}$$

The thickness of an individual model layer, k, is then the difference in geopotential height between its upper and lower boundaries: $\Delta Z_k = Z_{k+1} - Z_k$

Moreover, the NH_3 volume mixing ratio in each layer is converted to a number density (N_{NH3}, in molecules cm^{-3}), using the pressure and temperature of that specific model layer. Finally, the total NH_3 vertical column density (VCD, in molecules cm^{-2}) is calculated by integrating the vertical column density in each layer of the model. In our discrete model layers, this is achieved by summing the partial column of each layer, which is the product of the number density ($N_{NH3,k}$) and the layer thickness (ΔZ_k).

Table S1 List of the parameterizations adopted in the WRF-Chem model.

Options	Parameterization
Microphysics Option	Morrison 2-moment scheme
Longwave Radiation Option	RRTMG scheme
Shortwave Radiation Option	RRTMG scheme
Surface Layer Option	MM5 Monin-Obukhov scheme
photolysis schemes	Fast-J photolysis
gas-phase chemical mechanisms	SAPRC99 scheme
aerosol schemes	MOSAIC scheme

Table S2 Surface NH_3 observations used in this study (from Pan et al., 2018)

Stations	Location	latitude (°N)	longitude (°E)	Autumn ($\mu g\ m^{-3}$)	Winter ($\mu g\ m^{-3}$)	Spring ($\mu g\ m^{-3}$)	Summer ($\mu g\ m^{-3}$)	Annual ($\mu g\ m^{-3}$)
FQA	Fengqiu	35.0	114.6	19.2	14.3	12.8	21.1	16.8
LCA	Luancheng	37.9	114.7	21.9	17.2	17.5	20.7	19.3
YCA	Yucheng	37.0	116.6	21.3	12.8	10	45.2	22.3
TSM	Tainshan	36.3	117.1	3.3	2.8	5.6	3.8	3.9
XLM	Xinglong	40.4	117.6	3.6	0.9	6.1	5.1	3.9
YFS	Yangfang	40.2	116.1	6	4.1	6	11.9	7
CZS	Cangzhou	38.3	116.9	22	22.2	25.6	26	23.9
TJU	Tianjin	39.1	117.2	12.3	7.2	11	14.5	11.3
BJU	Beijing	40.0	116.4	16.6	7.2	14.9	16.3	13.7
BDI	Baoding	38.9	115.5	12.7	10.5	12.4	25.7	15.3
TGI	Tanggu	39.0	117.7	8.4	8	11.9	12.7	10.2
THL	Taihu	31.6	120.3	3.4	5.7	6.0	10.3	6.3
NJU	Nanjing	32.1	118.4	11.6	7.5	9.5	14.6	10.8

Table S3 List of meteorological observation stations in this study

Station	Code of sites	Longitude	Latitude
Beijing	54511	116.47 °E	39.80 °N
Tianjin	54527	117.05 °E	39.08 °N
Shijiazhuang	53698	114.35 °E	38.07 °N
Zhengzhou	57083	113.65 °E	34.72 °N
Jinan	54823	117.00 °E	36.60 °N
Shanghai	58362	121.45 °E	31.40 °N
Nanjing	58238	118.90 °E	31.93 °N
Hangzhou	58457	120.17 °E	30.23 °N
Hefei	58321	117.30 °E	31.78 °N

Table S4 List of air pollution observation sites in this study

Cities	The number of sites	Information of sites Code (longitude, latitude)
Beijing	12	1001A (116.366°E, 39.867°N) 1002A (116.170°E, 40.286°N) 1003A (116.434°E, 39.952°N) 1004A (116.434°E, 39.875°N) 1005A (116.473°E, 39.972°N) 1006A (116.361°E, 39.943°N) 1007A (116.315°E, 39.993°N) 1008A (116.720°E, 40.144°N) 1009A (116.644°E, 40.394°N) 1010A (116.230°E, 40.195°N) 1011A (116.407°E, 40.003°N) 1012A (116.225°E, 39.928°N)
Tianjin	9	1015A (117.145°E, 39.165°N) 1017A (117.237°E, 39.108°N) 1018A (117.202°E, 39.093°N) 1019A (117.184°E, 39.213°N) 1021A (117.307°E, 39.088°N) 1023A (117.707°E, 39.034°N) 1024A (117.457°E, 38.839°N) 1026A (117.764°E, 39.159°N) 1027A (117.157°E, 38.919°N)
Shijiazhuang	7	1029A (114.455°E, 38.051°N) 1030A (114.605°E, 38.040°N) 1031A (114.502°E, 38.140°N) 1032A (114.459°E, 38.006°N) 1033A (114.533°E, 38.018°N) 1034A (114.521°E, 38.052°N) 1035A (114.354°E, 37.910°N)
Zhengzhou	8	1316A (113.684°E, 34.762°N) 1317A (113.641°E, 34.775°N) 1318A (113.675°E, 34.802°N) 1320A (113.727°E, 34.719°N) 1321A (113.734°E, 34.719°N) 1322A (113.599°E, 34.750°N) 1323A (113.636°E, 34.754°N) 1324A (113.611°E, 34.916°N)
Jinan	8	1299A (116.988°E, 36.611°N) 1300A (116.930°E, 36.670°N) 1301A (117.114°E, 36.674°N) 1303A (117.068°E, 36.687°N) 1304A (116.943°E, 36.649°N) 1305A (117.049°E, 36.662°N) 1306A (116.734°E, 36.534°N) 1616A (117.679°E, 36.229°N)
Shanghai	8	1142A (121.478°E, 31.204°N) 1143A (121.467°E, 31.301°N) 1144A (121.412°E, 31.165°N) 1145A (121.536°E, 31.266°N) 1147A (121.425°E, 31.226°N) 1148A (121.703°E, 31.191°N) 1149A (121.533°E, 31.228°N) 1150A (121.577°E, 31.207°N)
Nanjing	9	1151A (118.803°E, 32.108°N) 1152A (118.749°E, 32.057°N) 1153A (118.778°E, 32.072°N) 1154A (118.777°E, 32.014°N) 1155A (118.803°E, 32.031°N) 1156A (118.795°E, 32.077°N) 1157A (118.626°E, 32.088°N) 1158A (118.737°E, 32.009°N) 1159A (118.907°E, 32.105°N)

Hangzhou	9	1223A (120.211°E, 30.210°N) 1224A (120.063°E, 30.275°N) 1226A (120.348°E, 30.306°N) 1227A (120.127°E, 30.246°N) 1228A (120.190°E, 30.269°N) 1230A (120.120°E, 30.312°N) 1231A (120.301°E, 30.418°N) 1232A (120.270°E, 30.182°N) 1233A (120.088°E, 30.181°N)
Hefei	10	1270A (117.196°E, 31.785°N) 1271A (117.307°E, 31.877°N) 1272A (117.259°E, 31.871°N) 1273A (117.160°E, 31.905°N) 1274A (117.250°E, 31.857°N) 1275A (117.266°E, 31.944°N) 1276A (117.336°E, 31.858°N) 1277A (117.302°E, 31.796°N) 1278A (117.278°E, 31.739°N) 1279A (117.124°E, 31.852°N)

Table S5 List of the evaluation metrics of NH_3 concentrations.

	The total column concentration (10^{15} molc cm^{-2})		Surface volume concentration (μg m^{-3})	
	Prior	Posterior	Prior	Posterior
Mean obs.	29.0		12.7	
Mean model.	17.4	23.7	6.3	9.4
IOA	0.72	0.91	0.57	0.65
MFB	-0.61	-0.30	-0.61	-0.19
RMSE	13.9	7.9	9.1	7.3

Table S6 Seasonal comparison of simulated and observed surface NH_3 concentrations ($\mu g\ m^{-3}$) and associated statistical metrics.

	MAM	JJA	SON	DJF
Prior surface NH_3 concentration ($\mu g\ m^{-3}$)	5.05	7.58	6.68	6.06
Observed surface NH_3 concentration ($\mu g\ m^{-3}$)	11.48	17.53	12.48	9.26
IOA	0.49	0.54	0.66	0.67
MFB	-0.79	-0.74	-0.54	-0.37
RMSE ($\mu g\ m^{-3}$)	8.29	13.06	7.64	5.76
	MAM	JJA	SON	DJF
Posterior surface NH_3 concentration ($\mu g\ m^{-3}$)	8.86	10.10	9.13	9.44
Observed surface NH_3 concentration ($\mu g\ m^{-3}$)	11.48	17.53	12.48	9.26
IOA	0.56	0.61	0.7	0.72
MFB	-0.24	-0.47	-0.19	0.12
RMSE ($\mu g\ m^{-3}$)	5.86	10.63	6.13	5.08

Table S7: Comparison of prior and posterior simulated surface concentrations with in-situ observations for major secondary inorganic aerosol components (sulfate, nitrate, and ammonium) in Beijing. All values are in μg m^{-3}.

	Prior simulation	Posterior simulation	observation
nitrate	8.82	9.59	9.44
ammonium	4.71	4.95	5.69
sulfate	5.81	5.84	7.74

Table S8 Model performance in predicting meteorological parameters

Cities		Annual mean			
		Simulation	Observation	IOA	MFB
Beijing	T	284.0 K	286.5 K	0.97	-0.01
	RH	46.0 %	53.8 %	0.73	-0.10
	P	1019.3 hPa	1014.3 hPa	0.93	0.00
Tianjin	T	285.6 K	286.7 K	0.97	0.00
	RH	41.5 %	58.2 %	0.66	-0.31
	P	1019.9 hPa	1018.0 hPa	0.96	0.00
Shijiazhuang	T	285.2 K	287.3 K	0.96	-0.01
	RH	42.7 %	61.7 %	0.67	-0.35
	P	998.1 hPa	1005.6	0.87	-0.01
Jinan	T	287.1 K	289.3 K	0.96	-0.01
	RH	55.0 %	65.5 %	0.72	-0.17
	P	1010.2 hPa	1004.8 hPa	0.92	0.01
Zhengzhou	T	284.4 K	288.4 K	0.95	-0.01
	RH	57.2 %	59.8 %	0.74	-0.06
	P	993.2 hPa	997.6 hPa	0.92	0.00
Shanghai	T	289.9 K	291.1 K	0.97	0.00
	RH	67.7 %	75.2 %	0.72	-0.14
	P	1019.1 hPa	1017.2 hPa	0.96	0.00
Nanjing	T	288.5 K	290.0 K	0.97	-0.01
	RH	72.1 %	76.0 %	0.78	-0.07
	P	1017.6 hPa	1013.4 hPa	0.94	0.00
Hangzhou	T	288.8 K	291.5 K	0.96	-0.01
	RH	74.3 %	78.1 %	0.74	-0.07
	P	1009.6 hPa	1012.2 hPa	0.96	0.00
Hefei	T	288.0 K	290.2 K	0.97	-0.01
	RH	73.3 %	78.9 %	0.77	-0.10
	P	1015.0 hPa	1014.1 hPa	0.97	0.00

Table S9 NH_3 emission reduction scenarios in this study. The following emissions are all from the posterior inventory.

Scenario	Agricultural emission reduction (%)	Non-agricultural emission reduction (%)
All-sec30	30	30
AGR30	30	/
non-AGR30	/	30
All-sec40	40	40
AGR40	40	/
non-AGR40	/	40
All-sec50	50	50
AGR50	50	/
non-AGR50	/	50
All-sec60	60	60
AGR60	60	/
non-AGR60	/	60

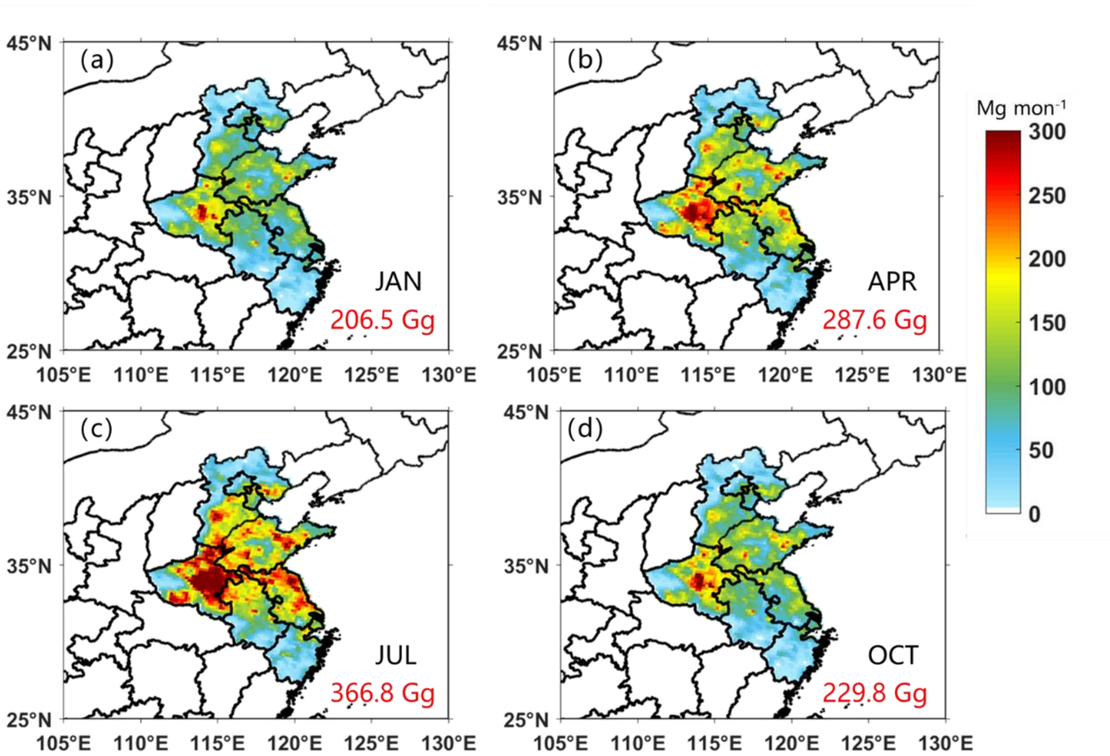

FigureS1. Distribution of prior NH_3 emissions in various months from MEIC. The red numbers show the total emissions over Eastern China.

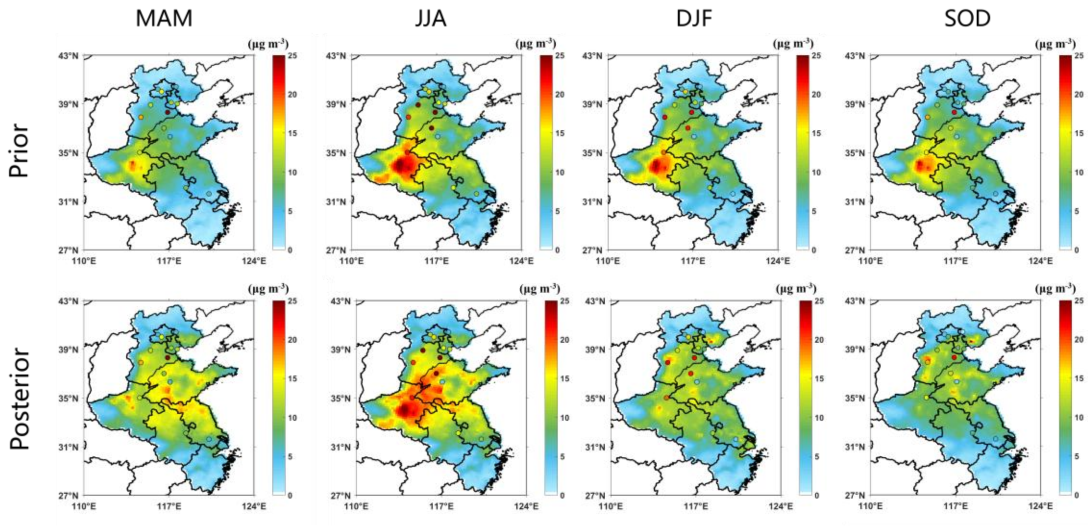

Figure S2. Distributions of surface posterior/prior NH_3 concentration and in-situ measurements scatters

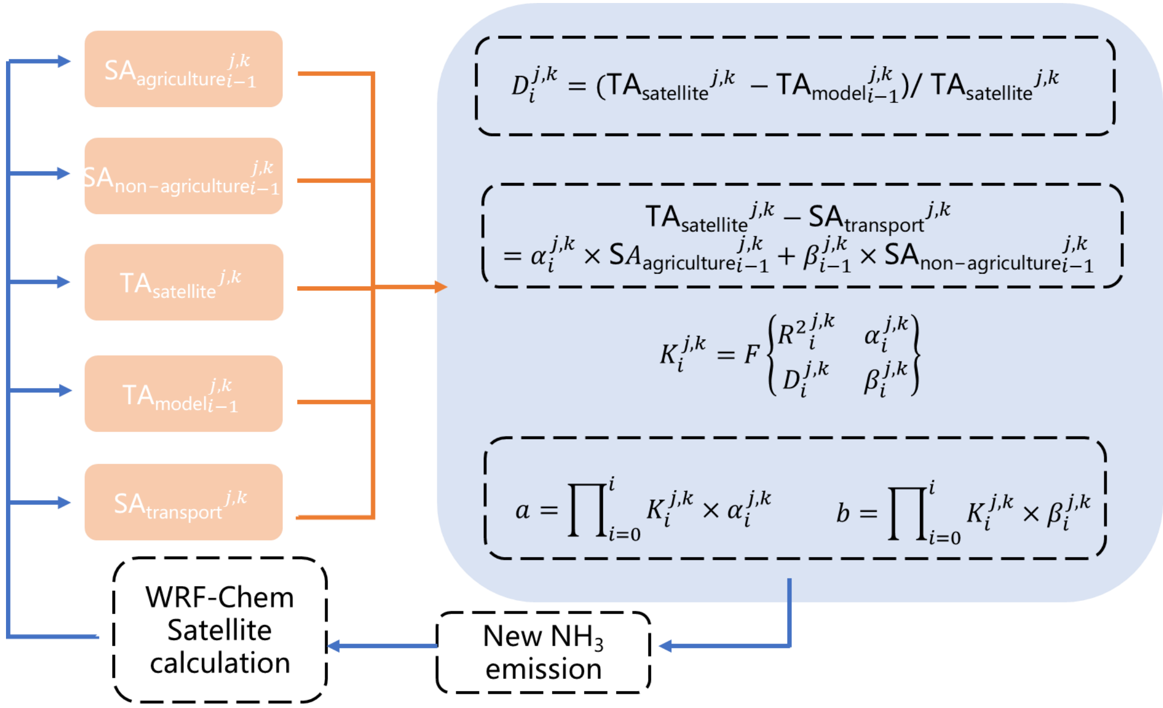

FigureS3. Visualization of the iterative algorithm process for NH_3 emission estimation

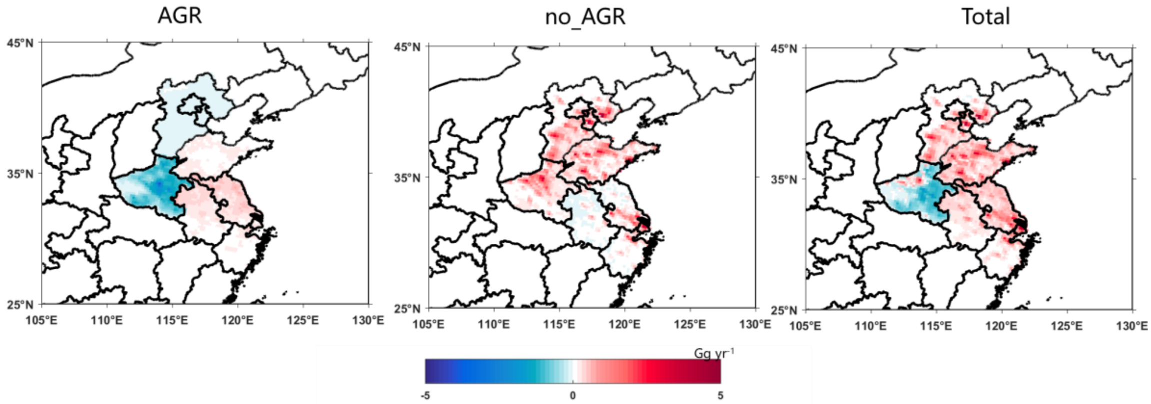

Figure S4. Spatial distribution of the difference in NH_3 emissions (Posterior − Prior) for AGR and non-AGR sources.

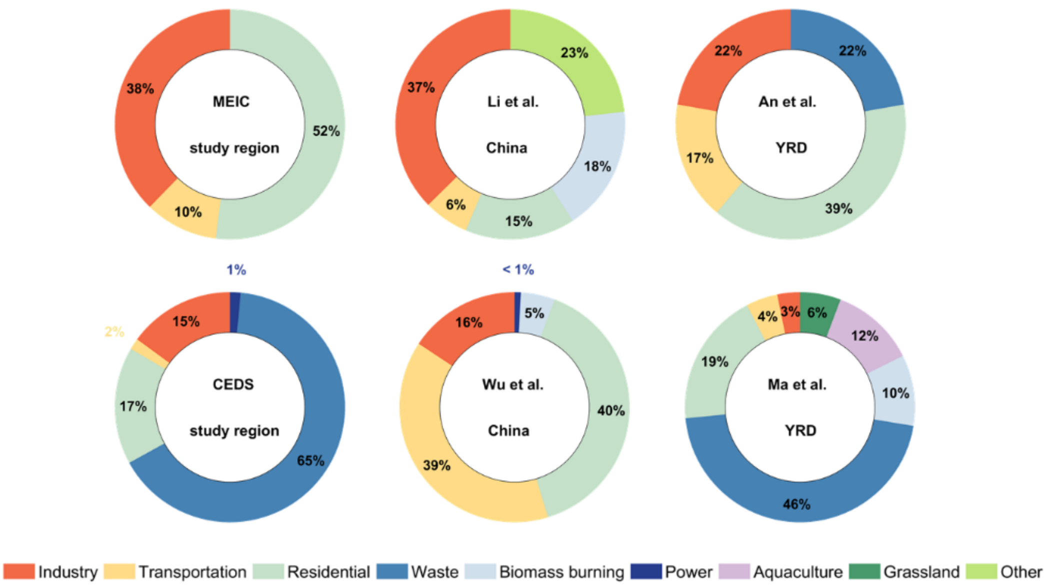

Figure S5. Comparison of the source apportionment of non-AGR NH_3 emissions from different studies and for various regions. Each pie chart illustrates the relative contribution (%) of nine specific non-agricultural sources, with the area (study region, China, and the YRD) and data source for each chart indicated in its center.

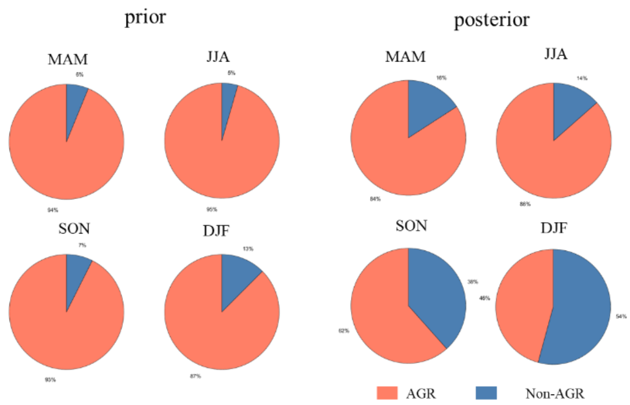

Figure S6. Seasonal comparison of prior and posterior NH_3 emissions from AGR and non-AGR sources.

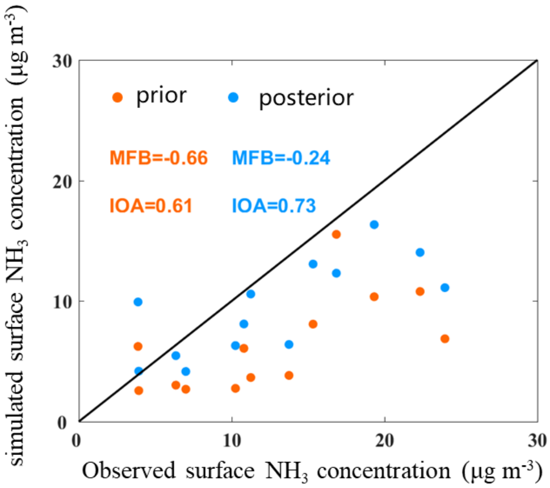

Figure S7. Scatter plot comparison of prior (orange) and posterior (blue) simulated seasonal mean surface NH_3 concentrations against in situ observations. The solid black line indicates the 1:1 ratio.

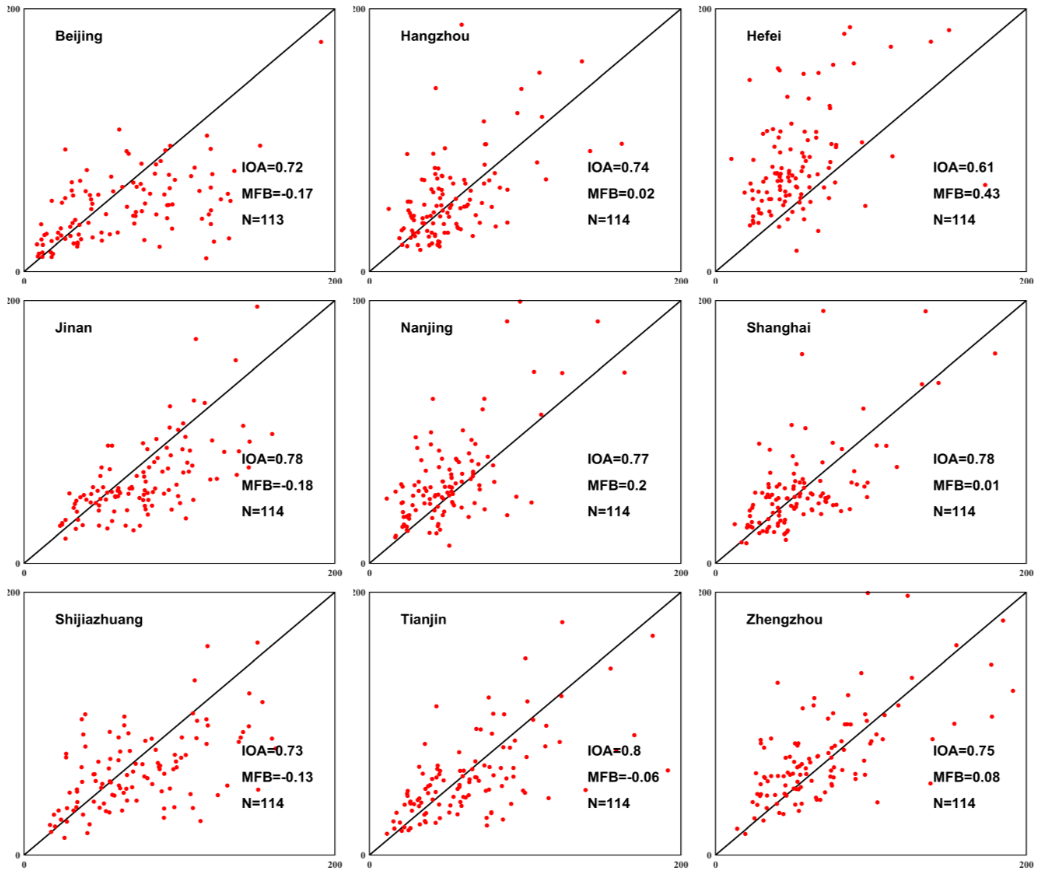

Figure S8. Scatters plot of simulation versus observation for daily $PM_{2.5}$ ($\mu g\ m^{-3}$).

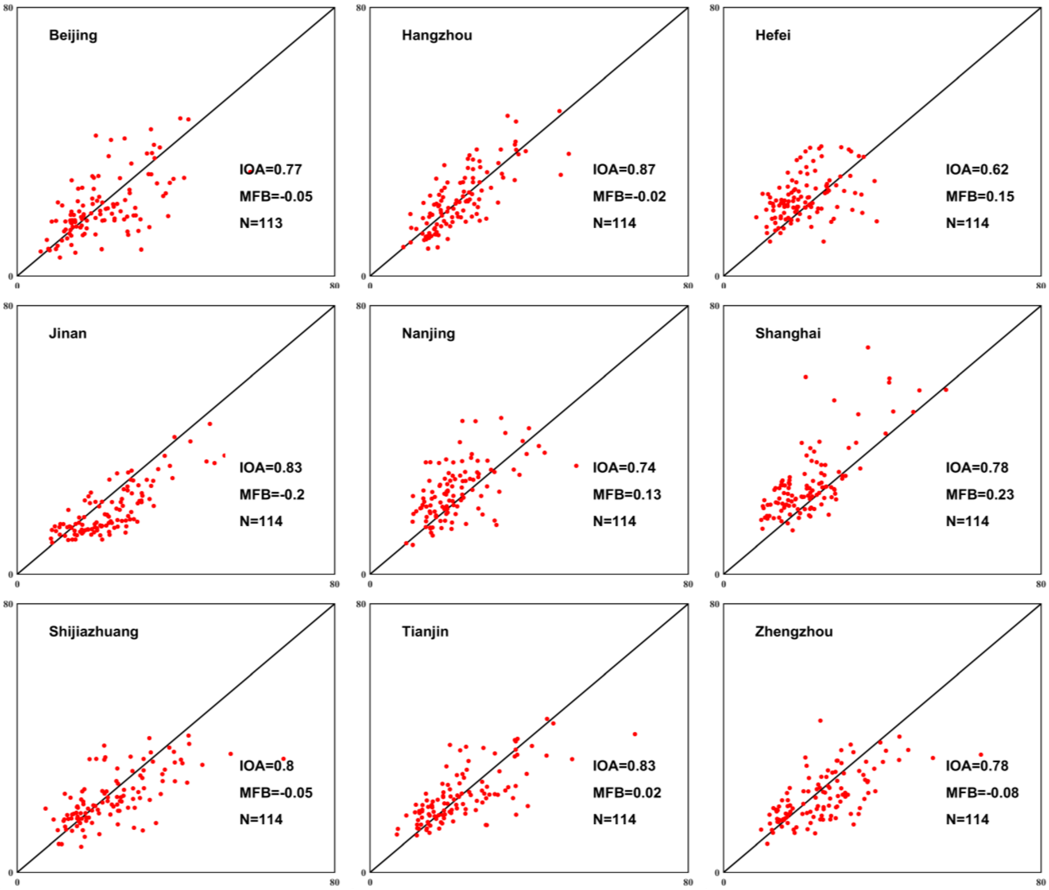

Figure S9. The same as Fig S6, but for NO_2 (ppbv).

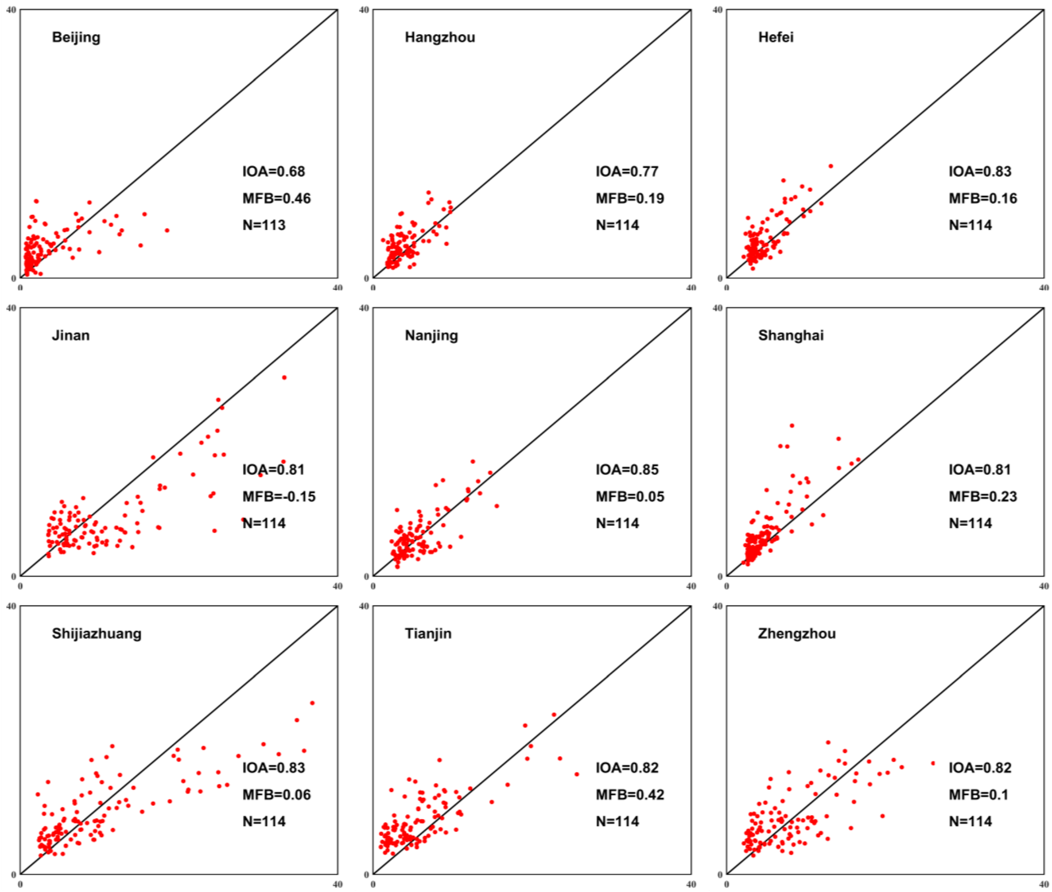

Figure S10. The same as Fig S6, but for SO_2 (ppbv).

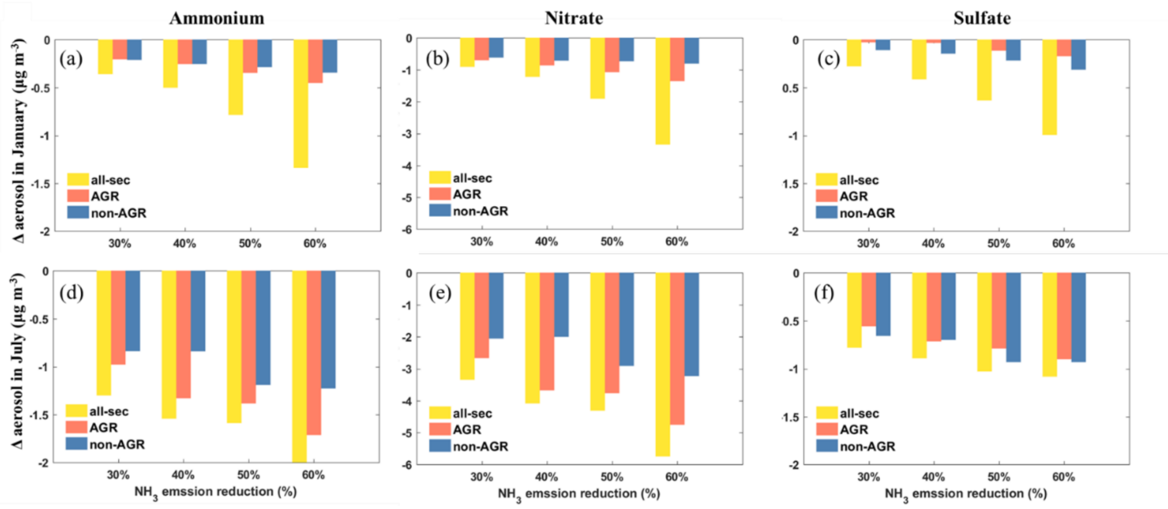

Figure S11. Response of particulate ammonium, nitrate and sulfate to NH_3 emission reduction.